Nanoscale

Accepted Manuscript

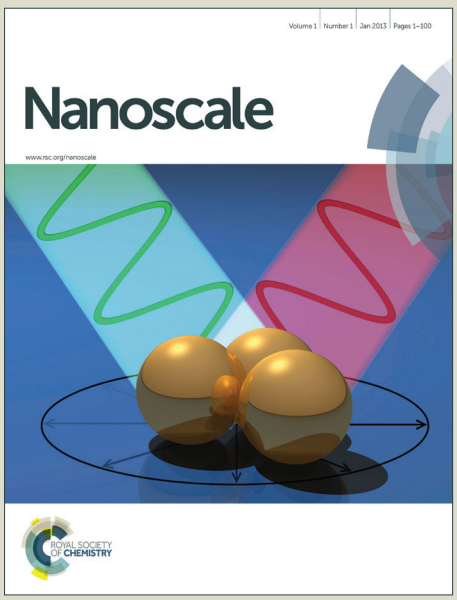

ROYAL SOCIETY OF CHEMISTRY

www.rsc.org/nanoscale

Nanoscale

ARTICLE

Wafer-scale graphene and ferroelectric multilayer for flexible and fast-switched modulation applications

Received 00th January 20xx,
Accepted 00th January 20xx

DOI: 10.1039/x0xx00000x

www.rsc.org/

Minmin Zhu,[ab] Jing Wu,[cd] Zehui Du,[e] Roland Yingjie Tay,[a] Hongling Li,[ab] Barbarous Özyilmaz,[cd] Edwin Hang Tong Teo*[ab]

Here we report wafer-scale Graphene/P(VDF-TrFE)/Graphene multilayer for light-weight, flexible and fast-switched broadband modulation applications. The P(VDF-TrFE) film not only significantly reduces the sheet resistance of graphene throughout heavy doping of ~ 0.8 x 10^{13} cm^{-2} by nonvolatile ferroelectric dipoles, but also acts as an efficient electro-optic (EO) layer. Such multilayer structure integration with remarkable ferroelectric polarization, high transparency (> 90%), low sheet resistance (~ 302 Ω/□), and excellent mechanic flexibility shows the potential of a flexible modulation application over a broad range of wavelength. Moreover, the derived device also exhibits strong field-induced EO modulation even under bending and one large pockels coefficient (~ 54.3 pm/V) is obtained. Finally, graphene and ferroelectric hybrid demonstrates a fast switching time (~ 2 μs) and works well below low sheet resistance level over a long time. This work gives insights into the potential of graphene and ferroelectric hybrid structure, enabling future explorations on next-generation high-performance, flexible transparent electronics and photonics.

Introduction

Currently there is growing interest in thin, lightweight, and flexible transparent electronics to meet the special needs for next-generation optic communications.[1,2,3] Graphene, which is considered as the strongest and thinnest material since its discovery,[4,5] exhibits a best known combination of high transparency, wideband tunability, and excellent mechanical strength that make it a promising candidate for ultrafast photodetectors,[6,7,8] tunable surface plasmon polariton[9,10,11] and broadband optical modulator devices.[12,13,14,15] Owing to its fine-structure constant ($e^2/\hbar c$),[12,16] graphene exhibits an ultrahigh transparency of up to 97.3%. Despite being only one atomic layer thick, the exceptionally strong covalent carbon-carbon bonds enable the intrinsic strength of graphene structure to reach as high as 1.0 TPa.[17] Combining graphene with silicon waveguides, one layer or few-layer graphene modulators with small footprint, low driving voltage, and low insertion loss have been exploited.[12,14,18] Although these graphene modulators demonstrate effective modulation of the guided light at frequencies over 1 GHz under ambient conditions by electrically tuning the Fermi level of the graphene,[12,19,20] almost they rely on Si-based waveguide structure whose footprint is in the order of millimeter due to the lower electro-optic effect of Si.[21] Moreover, these graphene modulators are rigid and not flexible due to the nature of silicon platform, which can't meet the increasing wearable market.[22] Finally, this type of graphene modulator still requires drastic performance improvement.[23] Thus, finding a replacement of the Si-based graphene modulator with a new candidate having adequate modulation speed and mechanic flexibility is not only of scientific interest but also industrial importance.

Another group of EO modulators based on complex perovskite-structured ferroelectric oxides, such as $Pb(Zr,Ti)O_3$ (PZT),[24,25] $(Pb,La)(Zr,Ti)O_3$ (PLZT),[26] and $(Ba,Sr)TiO_3$ (BST),[27] e.g., also faces a similar problem as they cannot be bent or rolled. Such EO modulators are based on tuning the polarization of ferroelectric films throughout the electric field; as a result, the operation principle is different from the graphene modulator which is based on blocking interband transition of graphene (Fermi Level).[12,28] In addition, fabricating these perovskite oxides generally requires a high deposition temperature (> 600 °C) and the formation of perovskite phase strongly depends on the substrate or seeding layer.[24,29,30] Therefore, new approaches with low temperature process (< 200 °C), improved performance, and simplified fabrication procedure are highly required. Recently, poly(vinylidene fluoride-co-trifluoroethylene) (P(VDF-TrFE) film integration with graphene has shown great potential in realization of superior stable, transparent and flexible electronics owing to its excellent

[a] School of Electrical and Electronic Engineering, Nanyang Technological University, 50 Nanyang Avenue, Singapore 639798.
[b] CINTRA CNRS/NTU/THALES, Nanyang Technological University, Research Techno Plaza, 50 Nanyang Drive, Singapore 637553.
[c] Graphene Research Center, National University of Singapore, 2 Science Drive 3, Singapore 117542.
[d] Department of Physics, National University of Singapore, 2 Science Drive 3, Singapore 117542.
[e] Temasek Laboratories, Nanyang Technological University, Research Techno Plaza, 50 Nanyang Drive, Singapore 637553.
† E-mail: htteo@ntu.edu.sg
Electronic Supplementary Information (ESI) available: See
DOI: 10.1039/x0xx00000x

optical transparency and mechanical flexibility.[31,32,33] Beyond the strong support for graphene film, it also exhibits remarkable polarization under the applied electric field, indicating the potential for electro-optic modulation application.[31] However, to date, no experimental studies on P(VDF-TFE) and graphene hybrids for flexible modulation application have been performed yet.

In this work, we present a new low-cost and solution-processed approach to fabricate wafer-scale graphene/P(VDF-TrFE)/graphene multilayer films for flexible modulation application. With the utilization of doping effect induced by polarization of P(VDF-TrFE) polymer, an equivalent doping concentration of 0.8×10^{13} cm^{-2} was realized, leading to a reduction of the sheet resistance of graphene from 696 Ω/□ down to ~ 302 Ω/□. Besides the enhancement of conductivity, the multilayer structure also provides an ideal combination of light weight, high transparency, and remarkable mechanical flexibility which make it a potential candidate for flexible modulation application. Finally, the switching time and performance stability of such modulator have also been discussed.

Experimental Section

Synthetic procedure

Large-area monolayer graphene films were deposited on a 25-μm Cu foil by a typical CVD process.[34] During the growth process, 10 sccm H_2 and 30 sccm CH_4 were input. The typical growth temperature and time were 1000 °C and 30 min, respectively. Subsequently, P(VDF-TrFE) solution using a dimethylformamide (DMF) as solvent was coated on the as-grown graphene on Cu foil. Graphene at back side was etched by oxygen plasma. To obtain high quality of crystalline P(VDF-TrFE) film, the sample was annealed in oven at 135 °C for 8h. The graphene film was wet-transferred on PET as target substrate for free-standing Gr/P(VDF-TrFE) film. Finally, the EO modulator based on Gr/P(VDF-TrFE)/Gr multilayer film was formed.

Characterization

X-Ray Diffraction (XRD), Fourier transform infrared spectroscopy (FTIR), Raman Spectroscopy, and Atom Force Microscopy (AFM) were used to identify and quantify the phases, doping level and surface morphology of the samples. The sheet resistance and *I-V* curve measurement were carried out at four probe station platform. The sheer resistance was calculated using the standard formula ($R_s = \pi R/\ln 2 \approx 4.53R$). The thickness and refractive index of P(VDF-TrFE) film were measured by surface profiler and ellipsometer. For optical characterization, the optical transparency was measured by the UV-Vis spectrometer. The EO setup was equipped with a He-Ne laser with the excitation wavelength at 632 nm.[25] Pulse generator and an amplifier provides hundreds-volts power supply (0 - 400 V) and high responsivity (~ 1 ns).

Results and discussion

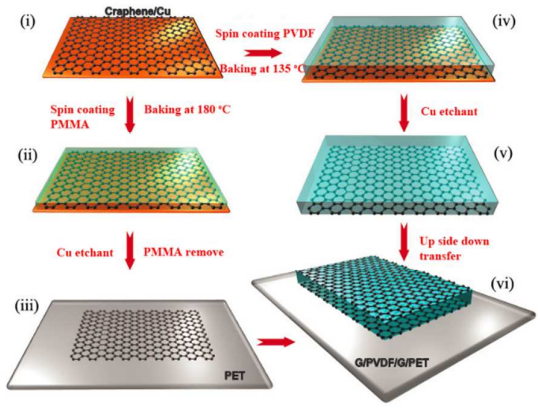

Fig. 1 Schematic illustration of electro-optic device fabrication based on Gr/P(VDF-TrFE)/Gr multilayer film. From (i) to (iii), device fabrication for Gr/PET electrode is illustrated. From (iv) to (vi), device fabrication of transferring Gr/P(VDF-TrFE) film on Gr/PET is shown.

Fig. 1 demonstrates the key steps to fabricate the EO modulator device based on P(VDF-TrFE) polymer sandwiched with graphene electrodes on polyethylene terephthalate (PET). All monolayer graphene samples were grown on 25-μm Cu foils by chemical vapor deposition (CVD) approach.[34] Wafer-scale CVD-grown graphene was first wet-transferred onto a PET film to be used as the bottom electrode (Fig. 1 (i-iii)). The size and the quality of monolayer graphene films can be refer to Fig. S1. It should be noted that graphene on PET demonstrates a small periodic modulation (0.1%) as a function of light polarization due to strain-induced optical anisotropy.[35] Such clear periodic modulation strongly hints at a state of uniaxial strain,[36] which is always accompanied by CVD-grown graphene due to polycrystalline copper substrate with diverse facets, grain boundaries, and annealing twins.[37] Fortunately, such adverse modulation of 0.1% can be eliminated by a Soleil-Babinet compensator when the modulator were tested.[25] Subsequently, P(VDF-TrFE) solution was coated on the another piece of graphene (which was still attached on Cu) by spin-coater and annealed in an oven at 135 °C for 8h to improve its crystallinity. A free-standing Gr/P(VDF-TrFE) film was achieved after removing the copper substrate in ammonium persulfate (APS) solution. Finally, Gr/P(VDF-TrFE)/Gr multilayer device was obtained by transferring the Gr/P(VDF-TrFE) film on G/PET through direct contact on the top side of the free-standing Gr/P(VDF-TrFE) films (Fig. 1 (iv-vi)).

The ferroelectric properties of the P(VDF-TrFE) films were then characterized as it plays a crucial role in the performance of the EO modulator devices and also affects the sheet resistance of the graphene films due to electrostatic doping effect. We first confirmed the thickness of the P(VDF-TrFE) film prepared with different spin speeds. When the spin speed was changed from 500 to 4000 rpm, the corresponding thickness of P(VDF-TrFE) films reduced from a few microns to hundreds nanometers (Fig. S2). It is noted that the polarization of thicker P(VDF-TrFE) films (500 rpm) needs higher voltage. Meanwhile, the thinner film (4000 rpm) is easily getting shorted by the driving voltage. Based on the measured thickness, the ferroelectric properties including remnant polarization (P_r) and coercive electric field (E_c) as a function of the film thickness are

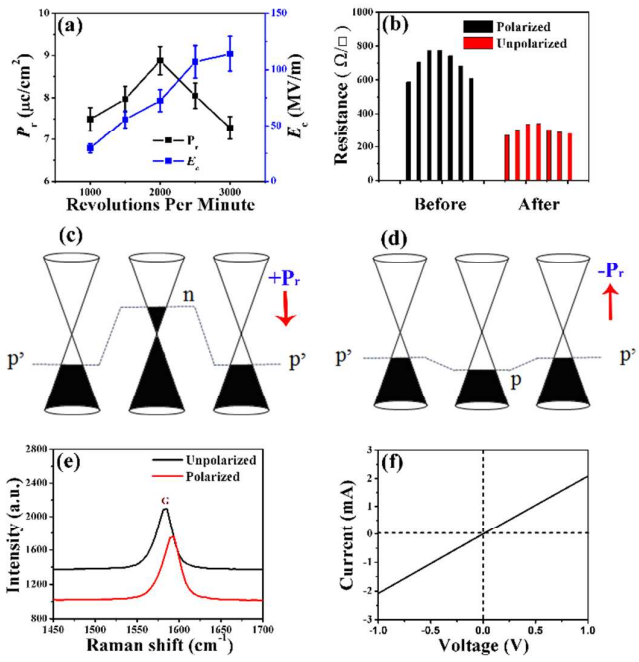

Fig. 2 (a) Remnant polarization (P_r) and coercive electric field (E_c) of P(VDF-TrFE) film as a function of spinning speed. (b) Sheet resistance of graphene film before and after polarization. Electrostatic doping in graphene with P(VDF-TrFE) film at the (c) + P_r and (d) -P_r state. After fully polarizing the ferroelectric films, the formation of p-n or p´-p´ junction in graphene can explain the change of sheet resistance. (e) Raman spectra of graphene on P(VDF-TrFE) film with and without pre-polarization. (f) *I-V* curve of wafer-scale Gr/P(VDF-TrFE) film.

compiled (Fig. 2a). We obtained a maximum P_r of 8.88 (μC/cm^2) when the film thickness is about 560 nm and its corresponding E_c is 72.3 (MV/m), which is much less than 575 (MV/m) of the breakdown filed (E_b) for P(VDF-TrFE) film.[38] Base on atomic force microscopy (AFM) analysis (Fig. S3), the surface roughness of P(VDF-TrFE) films is estimated to be 7 nm, which indicates that the ferroelectric films are smooth and homogeneous. With the optimal thickness of the P(VDF-TrFE) films for high P_r, we further study the effect of the ferroelectric dipoles of P(VDF-TrFE) films on the charge carrier density of graphene, thereby leading to the sheet resistance reduction after poling.[33] In total, seven locations (1.2 x 1.2 mm) were randomly chosen on Gr/P(VDF-TrFE) film to measure the sheet resistance. Fig. 2b shows the sheet resistance of graphene on the P(VDF-TrFE) film before and after poling. The mean sheet resistance of graphene on P(VDF-TrFE) film after poling is calculated to ~ 302 Ω/□, comparable to that of the graphene film grown in large pattern (280 Ω/□).[1] The unpoled samples have a mean value of ~ 696 Ω/□, about two time larger than that of poled one. The huge reduction of sheet resistivity implies that a doping effect may present in the graphene by polarized P(VDF-TrFE) polymer. Fig. 2c and 2d illustrate the electrostatic doping effect in graphene induced by P(VDF-TrFE) film under the positive and negative polarization state. As ferroelectric dipoles of P(VDF-TrFE) film are tuned to be the positive polarization (+P_r), the electrostatic n-type doping in graphene generates a random array of p-n junction, thereby leading to a large potential steps along the current direct (Fig. 2c). Therefore, the sheet resistance of graphene can be greatly enhanced. On the other side, we can obtain p-p' junctions under the -P_r state (Fig. 2d). Such p-p' junctions give rise to a smoother potential step, resulting in a much lower sheet resistance in graphene.[31,33] The doping level on graphene imposed by ferroelectric polymer can be easily determined by Raman spectroscopy, corresponding to the shift in G peak, which strongly depends on the level of doping.[39,40] Fig. 2e shows the Raman spectra of the as-prepared graphene films in which the G peak shifts around 9 cm^{-1} on the poled Gr/P(VDF-TrFE) film, corresponding to a doping concentration of ~ 0.8 × 10^{13} cm^{-2}.[40] At this doping level, the *I-V* measurements on wafer-scale Gr/P(VDF-TrFE)/Gr film yield a sheet resistance of ~ 471 Ω/□ (Fig. 2f). The value is slightly higher than 302 Ω/□ measured on a patterned sample size of 1.44 μm^2 due to the surface fluctuation and short poling process.[31] For the applications of Gr/P(VDF-TrFE) films in the wafer size, a lower sheet resistance is possible by further optimizing the transfer process and fabrication technique.[32] More importantly, both n-type and p-type doped graphene films integrating with ferroelectric P(VDF-TrFE) film can also be realized using the same procedure.

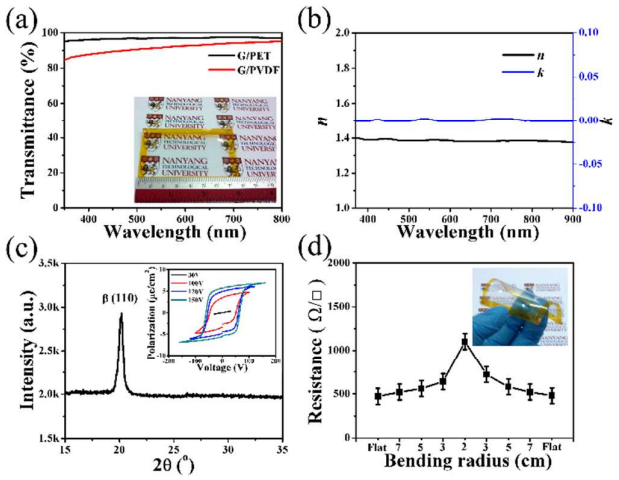

Fig. 3 (a) Transmittance spectra of Gr/P(VDF-TrFE)/Gr multilayer (> 90%) and pure graphene on PET (97%). The inset is optical image of Gr/P(VDF-TrFE)/Gr multilayer on transparent PET substrate. The background is the logo of Nanyang Technological University. (b) Refractive index (*n*) and the extinction coefficient (*k*) of P(VDF-TrFE) film as a function of wavelength. (c) Typical XRD pattern of P(VDF-TrFE) thin film indicating the formation of β phase. The inset is the polarization hysteresis loops of the Gr/P(VDF-TrFE)/Gr multilayer under different external voltages of 30, 100, 120, and 150 V. (d) Sheet resistance versus external strain using four probe bending measurement. The inset shows the optical image of Gr/P(VDF-TrFE)/Gr multilayer film device under bending.

Besides good polarization and remarkable conductivity, the optical properties (i.e. transparency, refractive index) and mechanical flexibility are equally critical for the applications of G/P(VDF-TrFE)/G films in flexible EO modulation devices. Fig. 3a shows the transmittance spectra of a monolayer graphene and Gr/P(VDF-TrFE)/Gr multilayer films. The inset shows the photograph of the transparent modulator device. Monolayer graphene exhibits ~ 97% transmission, while the multilayer EO device retained a very high transparency, slightly reducing to ~

93% at 632 nm. Such graphene and ferroelectric hybrids exhibits more than 90% transition from the visible to the near-infrared range, also indicating that one modulation device based on the graphene and P(VDF-TrFE) sandwiched structure can operate at a wild wavelength range. In order to extract the refractive index (*n*) of P(VDF-TrFE) film, the ellipsometric parameters Ψ and Δ of the film was plotted as a function of wave number (Fig. S4a). In the spectra, multiple reflections were observed which were induced by the interference of the light and are dependent on the thickness of the films. Fig. 3b shows the dependence of refractive index (*n*) and the extinction coefficient (*k*) with respect to the wavelength of the incident light. The extracted *n* at 632 nm is estimated to be ~ 1.4 and is slightly reduced over the visible to near-infrared wavelength range. The crystalline quality of P(VDF-TrFE) films was also investigated by X-ray diffraction (XRD) and Fourier transform infrared spectroscopy (FTIR). As shown in Fig. 3c, the XRD pattern of P(VDF-TrFE) film presents a single peak at 20°, implying the presence of β phase which possesses excellent ferroelectric property and fast discharge speed.[31,38] Meanwhile, FTIR result showed one unique peak (840 cm^{-1}), further confirming the presence of β phase again(Fig. S4b).[32] The inset of Fig. 3c demonstrates the typical hysteresis loops of Gr/P(VDF-TrFE)/Gr multilayer film in the ranges of ± 30, 100, 120, and 150V, corresponding to the polarization values of 0.3, 4.8, 5.9, and 7.0 μC/cm^2, respectively. The excellent polarization of ferroelectric films is critical for EO modulator operation which is based on the tuning of polarization. The value of ferroelectric polarization is also comparable to those observed in high quality P(VDF-TrFE) thin film.[31,37] Fig. 3d shows the mechanic foldability of the modulator device by measuring the sheet resistance of graphene under external strain. The inset displays the bending of a modulator device. The sheet resistance shows a small increase with increasing external bending radius of above 3 cm, and recovers after releasing the bending stress. The calculated bending strain varies between 0.03 and 0.394% (Fig. S5).[41] This result also suggests that such graphene on P(VDF-TrFE) film is a promising architecture for highly flexible applications. The graphene and ferroelectric hybrids with high optical transparency, low sheet resistance and outstanding mechanical flexibility provide a light weight and flexible transparent electronics platform for multifunctional optoelectronic applications, especially flexible EO modulation application.

The electric field induced optical modulation of the Gr/P(VDF-TrFE)/Gr devices was then characterized by a customized ellipsometric setup using a 632 nm He–Ne laser as light source (Fig. 4a).[25,42] The Gr/P(VDF-TrFE)/Gr devices with or without bending were mounted on a flat ceramics plate with an open aperture of 5 mm in diameter to allow laser to pass through (Fig. 4b and 4c). Based on the field-induced optical modulation, Pockels coefficient of P(VDF-TrFE) films can be extracted (see Supporting Information for a detailed description)[24,25] The angle of polarizer before and after the modulation device are +45° and -45°, respectively. In ideal conditions, there is no modulated light signal observed under zero electric field. As the electric field increases slowly, some laser intensity modulation is received by the photodetector. An insetting chopper was used to detect the modulation of laser intensity. To minimize the measurement error, a compensator was used to compensate the extra phase shift induced by the PET substrate, graphene film, and other optical accessories. Pulse generator and power amplifier with high responsivity (~ 1 ns) were installed in the setup to provide a large voltage range from 0 to 400 V.

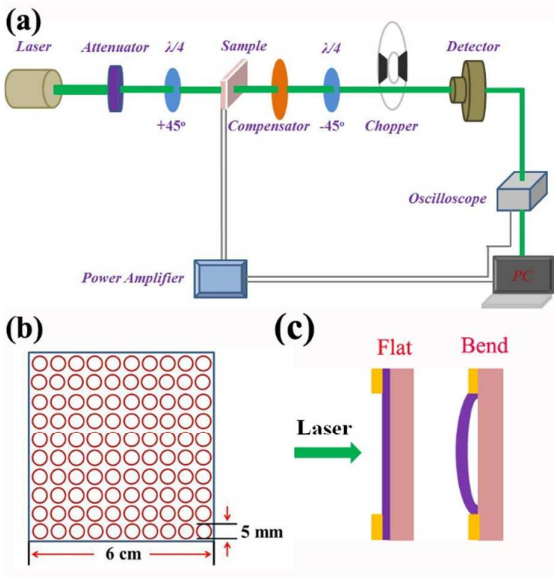

Fig. 4 (a) Experiment setup for electro-optic modulation measurement. (b) Ceramic-based sample holder with millimeter-size hole arrays. The diameter of each hole is 5 mm. (c) Schematic of Gr/P(VDF-TrFE)/Gr device for EO measurement under flat and bend status.

Fig. 5a shows the laser intensity modulated by the Gr/P(VF-TrFE)/Gr device under external applied voltage. When the flat modulator was tested, a strong field-induced optical modulation is observed using a driving voltage of tens of volts, indicating that our modulator device exhibits good work performance with a relatively low external voltage. The optical modulations were then compared between a flat state and a bent state. Under low applied voltage (20V), the modulated laser intensity of the bent device demonstrates a slightly higher value than that of the flat state (Fig. 5b inset). The small increase may arise from the effect of oxygen vacancy in ferroelectric material under the external stress field.[43] As the driving voltage further increases to 50 V, the modulated laser intensity significantly increases. The increased intensities are very close to each other for the device in flat and bending state (Fig. 5b). The result indicates that our modulator is equally functionable under a bending state almost without any loss of work performance. The inset of Fig. 5c summarizes the modulated laser intensity of the EO modulator as a function of driving voltage. The data for the device with and without bending are complied. From tens to hundreds volts, the modulator based on sandwiched Gr/(PVDF-TrFE)/Gr multilayer films exhibits an outstanding modulation performance as a function of the external voltage. Figure 5c reveals the change in birefringence (Δ*n*) as a function of the driving voltage. The relationships between birefringence (Δ*n*), phase shift (Δ*Φ*), and EO coefficient (r_{33}) are given by:

$$\Delta\emptyset = 2\pi L\Delta n/\lambda \quad (1)$$

$$r_{33} = (\lambda\Delta\emptyset)/(\pi n^3 EL) \quad (2)$$

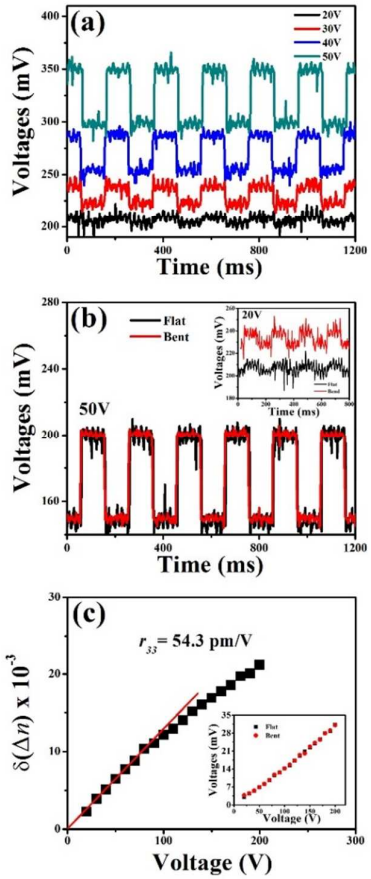

Fig. 5 (a) Laser intensity modulation of Gr/P(VDF-TrFE)/Gr multilayer film under different external applied voltage. (b) Laser intensity modulation of Gr/P(VDF-TrFE)/Gr multilayer with flat and bending status at 50 V. The inset is intensity modulation of multilayer structure with flat and bent status at 20 V. (c) Change in birefringence (Δn) as a function of applied voltage. The inset is modulation of Gr/P(VDF-TrFE)/Gr multilayer film with flat and bent status as a function of external applied voltage.

where $\Delta\Phi$ is the phase shift, L is the device length, Δn is the birefringence shift, λ is the laser wavelength, r_{33} is the Pockel coefficient, n is the refractive index, and E is the electric field. In our longitudinal EO modulator, L is also equal to the thickness of the P(VDF-TrFE) films. The pockels coefficient (r_{33}) of the P(VDF-TrFE) thin film is calculated to be ~ 54.3 pm/V, which is little higher than ~ 40 pm/V for P(VDF-TrFE) copolymer cured by electron irradiation or other methods.[44,45] The improvement on linear EO coefficient mainly arises from the excellent ferroelectric characteristics of P(VDF-TrFE) films with β phase. Meanwhile, the utilization of one-atom-thick graphene electrodes to replace conventional ITO may be another reason as graphene films effectively reduce the scattering and propagation loss of laser. Moreover, smooth and homogeneous surface really decrease the voids caused by roughness and porosity inside the film and may also responsible for the improved EO effects.[24,26] When we change the L from 550 μm (2000 rmp) nm to 1.2 μm (1000 rmp), the modulator also works well although the driving voltage significantly increased as the driving voltage is inversely proportional to the thickness of the P(VDF-TrFE) film (Fig. S6). Beyond electro-optic modulation application, such graphene and P(VDF-TrFE) multilayer films in principle directly serve as a nanogenerator or other optoelectronic devices.[32,41]

For electro-optic modulation applications, switching time and performance stability are two key factors for the large-scale industrial production. We measured the switching time of EO modulator by using a specially designed pulse generator and amplifier with an ultrafast response time (~ 1 ns). As the voltage changes from 50 to 150 V, the response of the switching time in EO setup shows a small change from 6 to 6.25 ns, which enable a highly precise measurement of the switching time of our modulation device (Fig. S7). As the external voltage of 50 V is applied on the Gr/P(VDF-TrFE)/Gr modulator, the switching time is ~ 2 μs (Fig. 6a). This value, although slightly more than the reported fastest charge/discharge time (~ 1 μs) of P(VDF-TrFE) films reported so far,[38] is still very promising since it can be further improved by optimizing the fabrication process and transfer technique. This finding indicates that such Gr/P(VDF-TrFE)/Gr modulator possesses a very fast switching time, which is also much better than that of other perovskite-structured complex oxides with kerr electro-optic effect (~ 3 - 6 μs), such as $Pb(Mg_{2/3}Nb_{1/3})O_3 – PbTiO_3$ (PMN-PT) film.[46]

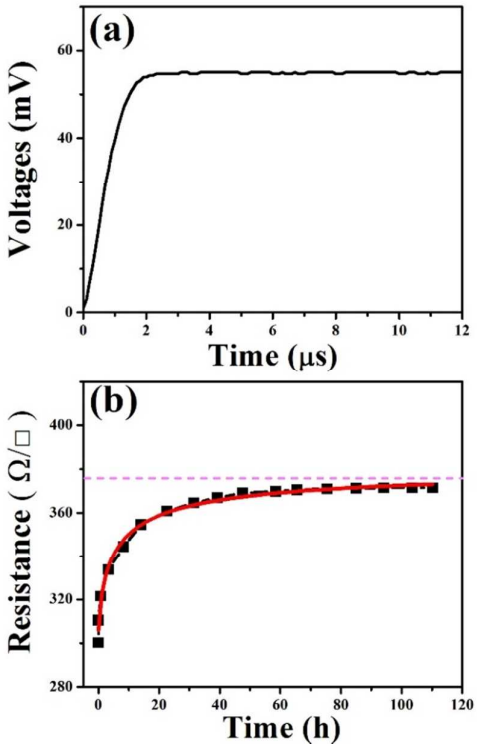

Fig. 6 (a) Switching time of modulator based on Gr/P(VDF-TrFE)/Gr multilayer film at 50 V. (b) Retention measurement of Gr/P(VDF-TrFE) film over 110 hours.

Long-term stability of low-resistance states in full-organic ferroelectrically gated graphene transistors is an essential prerequisite for electronic and photonic applications.[47,48] It is well known that the retention performance of ferroelectric field-effect transistors (FET) is determined by the charge injection and screening in the interface-adjacent layer. The charge injected and subsequently trapped at the interface screens the polarization and hence reduces the net

polarization that controls the channel resistance.[47] Fig. 6b illustrates the time-dependent sheet resistance of graphene on P(VDF-TrFE) film at zero gate bias. Given the P(VDF-TrFE) film under full polarized status, its ferroelectric dipoles are aligned along the external electric field direction. Throughout the retention measurement, the sheet resistance of the Gr/P(VDF-TrFE) film is continuously measured over 110 hours. The exponential decay of E_d vs. time is given by the following expression:[48]

$$E_d = \frac{V_g}{d} = C\ exp\left[\frac{-\alpha t}{\varepsilon_0 \varepsilon_d}\right] \quad (3)$$

Where E_d is the electric field in the passive layer, V_g is the back-gate voltage, C is a constant, ε_0 is dielectric permittivity of vacuum, ε_d is dielectric constant, and α is the linear constant (the injection current $J(E_d) = \alpha E_d$). For a fully polarized P(VDF-TrFE) film, the device follows a slow, logarithmic increase till saturation. Such an increase in our sample is generally due to the presence of an accidental interfacial layer between graphene and P(VDF-TrFE) film induced by wet transfer or spin-coating process. Thus, this adverse effect can be minimized by optimizing the wet transfer process or adopting an interface engineering.[2, 49,] Meanwhile, the sheet resistance of graphene in our device also displays a logarithmic behavior as the time changes, which also agrees well with the exponential decay in equation (3). Note that an extrapolation based on the fitting curve shows (red line), that even the sheet resistance of existing devices based on a wet transfer process would at most saturate to approximately 374 Ω/□ over the course of a year and will stay well below 420 Ω/□ over 5 years. Beyond the modulation applications, such graphene and ferroelectric hybrids also can directly serve as long-lasting and flexible transparent electrodes in light-emitting diodes photovoltaic and solar cell devices due to their high transparency, low sheet resistance, remarkable mechanic property, and long-term stability.[50,51,52]

Conclusions

In conclusion, we have reported a flexible and fast-switched electro-optic modulation application of wafer-scale graphene/P(VDF-TrFE)/graphene multilayer films. With the graphene and P(VDF-TrFE) films stacking together, the P(VDF-TrFE) film can induce a nonvolatile electrostatic doping to graphene and reduce its sheet resistance to half only (~ 302 Ω/□). Such multilayer films demonstrate a best combination of excellent conductivity, high transparency (> 90%), and mechanical flexibility, yielding a strong field-induced modulation even under bending. The derived modulation device also exhibits a linear EO behavior with Pockels coefficient of ~ 54.3 pm/V and a fast switching time (~ 2 μs). Finally, this device possesses a remarkable environmental stability and stays well below low sheet resistance level over a long time. Our work demonstrates a low-cost, facile, and scalable manner with solution-processed graphene and organic ferroelectric hybrids, providing a lightweight and flexible transparent electronics platform for next-generation photonic, plasmonics, and optoelectronic applications.

Acknowledgements

M. M. Zhu and J. Wu contributed equally to this work. The authors would like to acknowledge the funding support from NTU-A*STAR Silicon Technologies Centre of Excellence under the program grant No. 1123510003 and Singapore Ministry of Education Academic Research Fund Tier 2 No. MOE2013-T2-2-050.

Notes and references

1 K. S. Kim, Y. Zhao, H. Jang, S. Y. Lee, J. M. Kim, K. S. Kim, J. H. Ahn, P. Kim, J. Y. Choi and B. H. Hong, *Nature*, 2009, **457**, 706.
2 S. Bae, H. Kim, Y. B. Lee, X. F. Xu, J. S. Park, Y. Zheng, J. Balakrishnan, T. Lei, H. R. Kim, Y. I. Song, Y. J. Kim, K. S. Kim, B. Özyilmaz, J. H. Ahn, B. H. Hong and S. Lijima, *Nat. Nanotech.*, 2010, **5**, 574.
3 D. Kuzum, H. Takano, E. Shim, J. C. Reed, H. Juul, A. G. Richardson, J. D. Vries, H. Bink, M. A. Dichter, T. H. Lucas, D. A. Coulter, E. Cubukcu and B. Litt, *Nat. Commun.*, 2014, **5**, 5259.
4 A. K. Geim, *Science*, 2009, **324**, 1530.
5 G. H. Lee, R. C. Cooper, S. J. An, S. Lee, A. V. D. Zande, N. Petrone, A. G. Hammerberg, C. G. Lee, B. Crawford, W. Oliver, J. W. Kysar and J. Hone, *Science*, 2013, **340**, 1073.
6 X. M. Wang, Z. Z. Cheng, K. Xu, H. K. Tsang and J. B. Xu, *Nat. Photonic*, 2013, **7**, 888.
7 F. N. Xia, M. Thomas, Y. M. Lin, V. G. Alberto and P. Avouris, *Nat. Nanotech.*, 2009, **4**, 839.
8 C. H. Liu, Y. C. Chang, T. B. Norris and Z. Zhong, *Nat. Nanotech.*, 2014, **9**, 273.
9 L. Ju, B. S. Geng, J. Horing, C. Girit, M. Martin, Z. Hao, H. A. Bechtel, X. G. Liang, A. Zettl, Y. R. Shen and F. Wang, *Nat. Nanotech.*, 2011, **6**, 630.
10 F. Bonaccorso, Z. Sun, T. Hasan and A. C. Ferrari, *Nat. Photonics*, 2010, **4**, 611.
11 V. W. Bara, M. S. Jang, M. Sherrott, J. L. Lopez and H. A. Atwater, *Nano Lett.*, 2013, **13**, 2541.
12 M. Liu, X. B. Yin, U. A. Erick, B. S. Geng, Z. Thomas, L. Ju, F. Wang and X. Zhang, *Nature*, 2011, **474**, 64.
13 S. R. Berardi, R. S. Yan, M. K. Michelle, T. Tang, T. Kristof, W. S. Hwang, J. Debdeep, L. Liu and H. G. Xing, *Nat. Commun.*, 2012, **3**, 780.
14 M. Liu, X. B. Yin and X. Zhang, *Nano Lett.*, 2012, **12**, 1482.
15 E. O. Polat and C. Kocabas, *Nano Lett.*, 2013, **13**, 5851.
16 R. R. Nair, P. Blake, A. N. Grigorenko, K. S. Novoselov, T. J. Booth, T. Stauber, N. M. R. Peres and A. K. Geim, *Science*, 2008, **320**, 1308.
17 C. G. Lee, X. D. Wei, J. W. Kysar and J. Hone, *Science*, 2008, **321**, 385.
18 Y. Nathan, A. Yoska, R. Ma, J. K. Steven and M. Li, *Nano Lett.*, 2014, **14**, 2741.
19 Q. L. Bao and K. P. Loh, *ACS Nano*, 2012, **6**, 3677.
20 A. N. Grigorenko, M. Poloni and K. S. Novoselov, *Nat. Photonics*, 2012, **6**, 749.
21 K. Kim, J. Y. Choi, T. Kim, S. H. Cho and H. J. Chung, *Nature*, 2011, **479**, 338.
22 M. Tamagnone, A. Fallahi, J. R. Mosig and J. P. Carrier, *Nat. Photonics*, 2014, **8**, 556-563.
23 M. Tamagnone, A. Fallahi, J. R. Mosig, J. P. Carrier, Nat. Photonics 2014, 8, 556.
24 M. M. Zhu, Z. H. Du, J. Ma, *J. Appl. Phys.*, 2010, **108**, 113119.
25 M. M. Zhu, Z. H. Du, L. Jing, Alfred I. Y. Tok, Edwin H. T. Teo, *Appl. Phys. Lett.*, 2015, **107**, 031907.
26 Z. H. Du, M. M. Zhu, J. Ma, *J. Appl. Phys.*, 2009, **105**, 061612.

27 D. Y. Wang, S. Li, H. L. W. Chan and C. L. Choy, *Appl. Phys. Lett.*, 2010, **96**, 061905.
28 E. J. Lee, S. Y. Choi, H. Jeong, N. H. Park, W. Yim, M. H. Kim, J. K. Park, S. Son, S. Bae, S. J. Kim, K. Lee, Y. H. Ahn, K. J. Ahn, B. H. Hong, J. Y. Park, F. Rotermund, D. I. Yeom, *Nat. Commun.*, 2015, **6**, 6851.
29 M. M. Zhu, Z. H. Du, J. Ma, *J. Appl. Phys.*,2009, **106**, 023113.
30 W. W. Bruce, *Annu. Rev. Mater. Res.*, 2007, **37**, 659.
31 G. X. Ni, Y. Zheng, S. Bae, C. Y. Tan, K. Orhan, J. Wu, B. H. Hong, K. Yao and B. Özyilmaz, *ACS Nano*, 2012, **6**, 3935.
32 S. H. Bae, K. Orhan, K. S. Bhupendra J. G. Kwon, J. C. Hyoung, B. Özyilmaz and J. H. Ahn, *ACS Nano*, 2013, **7**, 3130.
33 Y. Zheng, G. X. Ni, C. T. Toh, C. Y. Tan, K. Yao and B. Özyilmaz, *Phys. Rev. Lett.*, 2010,**105**,166602.
34 X. S. Li, W. W. Cai, J. H. An, S. Kim, J. Nah, D. X. Yang, R. Piner, V. Aruna, I. Jung, E. Tutuc, S. K. Banerjee, L. Colombo and R. S. Ruoff, *Science*, 2009, **324**, 1312.
35 G. X. Ni, H. Z. Yang, W. Ji, S. J. Baek, C. T. Toh, J. H. Ahn, V. M. Pereira and B. Özyilmaz, *Adv. Mater.*, 2014, **26**, 1081.
36 V. M. Pereira, R. M. Ribeiro, N. M. R. Peres and A. H. Castro Neto, *Europhys. Lett.*, 2010, **92**, 67001.
37 J. D. Wood, S. W. Schmucher, A. S. Lyons, E. Pop and J. W. Lyding, *Nano Lett.*, 2011, **11**, 4547.
38 B. J. Chu, X. Zhou, K. L. Ren, B. Neese, M. R. Lin, Q. Wang, F. Nauer and Q. M. Zhang, *Science*, 2006, **313**, 334.
39 M. Lazzeri and F. Mauri, *Phys. Rev. Lett.*, 2006, **97**, 266407.
40 A. Das, S. Pisana, B. Chakraborty, S. Piscanec, S. K. Saha, U. V. Waghmare, K. S. Novoselov, H. R. Krishnamurthy, A. K. Geim, A. C. Ferrari, and A. K. Sood, *Nat. Nanotech.*, 2008, **3**, 210.
41 J. H. Lee, K. Y. Lee, B. Kumar, N. T. Tien, N. E. Lee, S. W. Kim, *Energy Environ. Sci.*, 2013, **6**, 169.
42 Y. L. Lu, J. J. Zheng, M. C. Golomb, F. L. Wang, H. Jiang and J. Zhao, *Appl. Phys. Lett.*, 1999, **74**, 3764.
43 S. Srinoi, R. Yimnirun and Y. Laosiritaworn, *Ferroelectrics*, 2014, **470**, 35.
44 S. Z. Yin, Q. M. Zhang, K. W. Chung, R. Yang, Z. Y. Cheng and Y. Lu, *Opt. Eng.*, 2000, **39**, 670.
45 D. Y. Jeong, *J. Kor. Phys. Soc.*, 2004, **44**, 1527.
46 M. M. Zhu, X. L. Chen, Z. H. Du and J. Ma, *AIP Advances*, 2011, **1**, 042163.
47 R. Gysel, I. Stolichnov, A. K. Tagantsev, S. W. E. Riester, N. Setter, G. A. Salvatore, D. Bouvet and A. M. Ionescu, *Appl. Phys. Lett.*, 2009, **94**, 263507.
48 S. Raghavan, I. Stolichnov, N. Setter, J. S. Heron, M. Tosun and A. Kis, *Appl. Phys. Lett.*, 2012, **100**, 023507.
49 E. O. Polat, B. Osman and C. Kocabas, *Sci. Rep.*, 2014, **4**, 6484.
50 N. Li, S. Oida, G. S. Tuleski, S. J. Han, J. B. Hannon, D. K. Sadana and T. C. Chen, *Nat. Commun.*, 2013, **4**, 2294.
51 T. H. Han, Y. B. Lee, S. H. Choi, S. H. Bae, B. H. Hong, J. H. Ahn and T. W. Lee, *Nat. Photonics*, 2012, **6**, 105.
52 Z. Y. Yin, J. X. Zhu, Q. Y. He, X. H. Cao, C. L. Tan, H. Y. Chen, Q. Y. Yan, H. Zhang, *Adv. Energy Mater.*, 2014, **4**, 1300574.